PHYSICAL REVIEW D **96,** 055012 (2017)

Dark-photon searches via ZH production at e^+e^- colliders

Sanjoy Biswas,[1] Emidio Gabrielli,[2,3,4] Matti Heikinheimo,[5] and Barbara Mele[6]
[1]*Korea Institute for Advanced Study, 85 Hoegi-ro, Seoul 02455, Republic of Korea*
[2]*Dipartimento di Fisica, Theoretical Section, Università di Trieste, Strada Costiera 11, I-34151 Trieste, Italy*
[3]*INFN, Sezione di Trieste, Via Valerio 2, I-34127 Trieste, Italy*
[4]*NICPB, Rävala 10, Tallinn 10143, Estonia*
[5]*Helsinki Institute of Physics, University of Helsinki, P.O. Box 64, Helsinki FI-00014, Finland*
[6]*INFN, Sezione di Roma, P. le A. Moro 2, I-00185 Rome, Italy*
(Received 23 April 2017; published 12 September 2017)

We study the ZH associated production followed by the Higgs $H \to \gamma\bar{\gamma}$ decay into a photon plus an *invisible* and *massless* dark photon, at future high-energy e^+e^- facilities. Large $H \to \gamma\bar{\gamma}$ decay rates (with branching ratios up to a few percent) are allowed, thanks to possible nondecoupling properties of the Higgs boson under specific conditions, and unsuppressed dark-photon couplings in the dark sector. Such large decay rates can be obtained in the framework of recent flavor models that aim to naturally explain the observed spread in the fermion mass spectrum. We analyze the experimental prospects for observing the $e^+e^- \to ZH$ process followed by the semi-invisible Higgs decay into a photon plus a massless invisible system. Search strategies for both the leptonic and the hadronic final states (arising from $Z \to \mu^+\mu^-$ and $Z \to q\bar{q}$, respectively) are outlined. We find that a 5σ sensitivity to a branching fraction $BR_{\gamma\bar{\gamma}} \sim 3 \times 10^{-4}$ can be achieved by combining the two channels with an integrated luminosity of 10 ab^{-1} at a c.m. energy of 240 GeV. This is considerably better than the corresponding sensitivity in alternative channels previously studied at lepton colliders. The analysis is model independent, and its results can be straightforwardly applied to the search for any Higgs two-body decay into a photon plus an undetected light particle.

DOI: 10.1103/PhysRevD.96.055012

I. INTRODUCTION

The Higgs-boson discovery at the LHC in 2012 [1] marked a milestone in our understanding of the electroweak symmetry breaking via the Higgs-Englert-Brout mechanism [2]. Present data are consistent with the Standard Model (SM) expectations for the Higgs boson properties [3], although there is still room, especially in the Higgs sector, for potential new physics (NP) effects, which could be detected in the forthcoming collider physics program. NP could for instance affect the chiral symmetry breaking, which is parametrized in the SM by the Higgs Yukawa couplings to fermions, and is responsible for the fermion mass spectrum, flavor mixing and CP violating phenomena, whose pattern is presently in excellent agreement with experiments. Despite that, the origin of Yukawa couplings is actually a mystery. Their eigenvalues span over six orders of magnitude for charged fermions and even more if neutrinos have Dirac masses. Such an unexplained wide range of masses is often referred to as the flavor hierarchy problem. Indeed, it is not yet clear whether the Yukawa couplings are fundamental constants (like gauge couplings), arising for instance from an ultraviolet (UV) completion of the SM, or are just low-energy effective couplings. Although the latter possibility is presently the most promising to explain the origin of the fermion mass hierarchy, it could require the existence of a nontrivial NP structure able to give rise to the effective Yukawa couplings. For instance, hidden or dark sectors beyond the SM could do the job, by promoting the Higgs boson to the role of a portal to the dark sector.

On the other hand, general consensus is growing around the idea that a dark sector, weakly coupled to the SM, could be responsible for the observed dark matter (DM) in the Universe [4,5]. The dark-sector internal structure and interactions could include light or massless $U(1)$ gauge bosons (the dark photons) which mediate long-range forces between dark particles [6–9]. In cosmology, dark photons may help to solve the problems related to the small-scale structure formation [7], and, if massless, they can predict dark discs of galaxies [8]. On the theoretical side, scenarios with dark (or hidden) photons have been extensively investigated in the literature (especially in the framework of UV completions of the SM theory), both for massive and massless dark photons [10,11]. This has also motivated dedicated experiments [12], mainly focused on massive dark-photon searches though [13]. Recently, there has been a renewed interest for viable cosmological scenarios with DM that is charged under a $U(1)$ gauge group in the dark sector, decoupled from SM forces, and mediated by massless dark photons [14]. Constraints on DM charged under $U(1)$ interactions have been revisited, allowing for viable unexplored cosmological models with large couplings in the dark sector.

A NP theoretical flavor framework, aiming to solve not only the flavor hierarchy problem but also the origin of DM, has been proposed in [15]. The model can predict an exponential spread in effective Yukawa couplings, and is based on an unbroken $U(1)$ gauge symmetry in a dark sector, providing a theoretical explanation for the existence of long-range dark interactions, as suggested by cosmological observations [16–18]. The dark sector of the model contains a set of massive dark fermions (heavier SM-fermion replicas), which are SM singlet but are charged under the dark $U(1)$ gauge group. Furthermore, heavy messenger scalar fields, charged under both the dark $U(1)$ and the SM gauge group, are needed to transfer at one loop the flavor and chiral symmetry breaking from the dark sector to the SM fermions. Incidentally, although the theory is not supersymmetric, the messenger fields have the same SM quantum numbers as squarks and sleptons in minimal supersymmetric models [19].

The main paradigm of the Gabrielli-Raidal flavor model (GRFM) in [15] is that the Yukawa couplings are, rather than fundamental constants, effective low-energy couplings generated radiatively by the interactions in the hidden sector of the theory. In particular, Yukawa couplings are assumed to vanish at tree level by some symmetry (for a gauge-symmetry realization, see [20]), and are induced at one loop by dark-sector fields [15]. Due to chirality, Yukawa couplings follow the dark-fermion mass hierarchy, which in the GRFM is exponential. Indeed, the dark-fermion exponential spectrum is generated by a nonperturbative dynamics in the dark sector involving $U(1)$ gauge interactions. Then, since the $U(1)$ gauge symmetry is exact, the dark fermions have to be stable, and therefore are potential DM candidates. Then, the GRFM can provide a basis for a viable charged DM scenario, as, for instance, the one suggested in [14].

We stress that in the GRFM the observed quark and lepton spectrum can be reproduced up to a few percent by the exponential-spread relation for the dark-fermion masses [15,20,21], provided dark-fermion $U(1)$ charges of the same order are assumed. Moreover, the corresponding $U(1)$ fine structure constant can be predicted from the lepton mass-spectrum sum rules to be quite strong, although still within the perturbative regime [15,20,21]. Notice that one is indeed allowed to have a strongly coupled dark photon in the dark sector only for massless dark photons, which can be fully decoupled at tree level from the SM quark and lepton sector [10]. In fact, most of the present astrophysical and accelerator constraints apply to *massive* dark-photon couplings [12], for which *unavoidable* tree-level dark-photon couplings to SM matter fields arise [10].

Although it can be fully decoupled at tree level from SM particles, a massless dark photon can still have effective low-energy interactions with SM fields arising from higher dimensional operators, with the latter suppressed by a characteristic scale related to the mass of the messenger fields running in the loops. For example, a massless dark photon ($\bar{\gamma}$) can appear in the flavor changing neutral current (FCNC) $f \to f'\bar{\gamma}$ decays of the SM fermions [22], that are mediated by FCNC magnetic-dipole-type operators suppressed by the NP scale running in the loop.

On the contrary, dark-photon couplings to the Higgs boson can show nondecoupling properties (a typical example is when the messenger fields have the same quantum numbers as squarks and sleptons [23]). An effective gauge-invariant low-energy $H\gamma\bar{\gamma}$ interaction can indeed arise at one loop. This interaction is induced by a gauge-invariant dimension-5 operator, suppressed by an effective scale $\Lambda_{\rm eff}$, according to

$$\mathcal{L} = \frac{1}{\Lambda_{\rm eff}} H F_{\mu\nu} \bar{F}^{\mu\nu}, \tag{1}$$

where $F_{\mu\nu}$ and $\bar{F}_{\mu\nu}$ are the field strengths of the photon and dark photon, respectively. The effective high-energy scale $\Lambda_{\rm eff}$, as defined in Eq. (8) of [23], is

$$\Lambda_{\rm eff} = \frac{6\pi v}{R\sqrt{\alpha\bar{\alpha}}} \frac{1-\xi^2}{\xi^2}, \tag{2}$$

where v is the SM Higgs vacuum expectation value (VEV), $\xi \equiv \Delta/\bar{m}^2$ is the mixing parameter, $\Delta = v\mu$ is the off-diagonal term appearing in the left-right messenger square-mass matrix, $\bar{m}$ is the average messenger mass, and α and $\bar{\alpha}$ are the electromagnetic and $U(1)$ dark fine-structure constants, respectively. R is given by a product of quantum charges [see for instance Eq. (4) in [23] for notations]. The scale μ is connected to the VEV of a heavy singlet scalar field needed to generate effective Yukawa couplings at one loop [15]. Importantly, the ξ parameter can be viewed as a relative square-mass difference of the messenger mass eigenstates running in the loop [$m_\pm^2 = \bar{m}^2(1 \pm \xi)$], and should be positive and limited by 1, in order to avoid tachions in the spectrum. As we can see from Eq. (2), a nondecoupling limit can be realized when Δ and $\bar{m}^2$ grow simultaneously to large values, by keeping the ξ ratio nonvanishing. Under this requirement, Eq. (2) shows that the scale $\Lambda_{\rm eff}$ has a nondecoupling behavior, being proportional to the Higgs VEV as $\Lambda_{\rm eff} \sim \mathcal{O}(v/\xi^2)$. It can then potentially lead to observable effects even in the case of a heavy messenger sector [23], since in the GRFM typically one has $\xi\sim$ a few tens percent. Furthermore, we assume that the lightest messenger mass m_- satisfies the lower bound $m_- \gtrsim 2$ TeV, in order to avoid a conflict with present collider limits on the direct search of new colored particles. This also guarantees the validity of the low-energy approximation in the effective Lagrangian of Eq. (1).

An unsuppressed Higgs-boson coupling to a photon and a dark photon $H\gamma\bar{\gamma}$ in the Lagrangian in Eq. (1) could then provide a privileged way to search for dark photons via Higgs production at colliders, and subsequent $H \to \gamma\bar{\gamma}$ decay. In this paper, we consider the case of a massless dark photon, that from a phenomenological point of view is

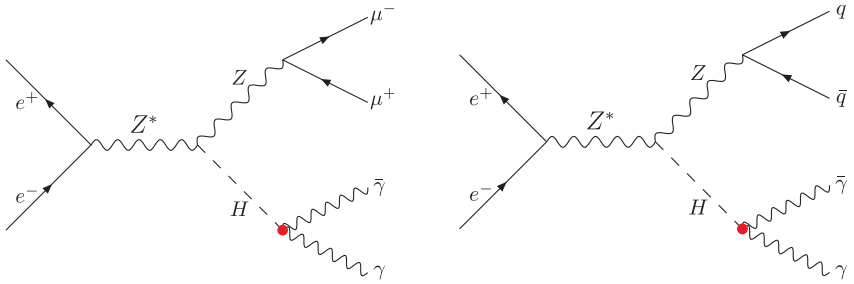

FIG. 1. Feynman diagrams for $e^+e^- \to ZH \to (\mu^+\mu^-, q\bar{q})(\gamma\bar{\gamma})$.

anyhow equivalent to a very light dark photon, which escapes detection by a typical collider apparatus.

A model-independent (parton-level) analysis of Higgs production via $gg \to H$ at the LHC as a mean for searching for massless dark photons has been presented in [23] for a LHC c.m. energy of 8 TeV. More recently, an improved study (including parton-shower effects) with a c.m. energy upgraded to 14 TeV was done in [24], where both the gluon-fusion and the vector-boson-fusion (VBF) production mechanisms have been considered. A crucial point is that, since the on-shell massless dark photon can be fully decoupled from SM fermions at tree level [10], it is characterized by a neutrinolike signature in a normal collider detector. After its production in collisions, it can then be revealed only by a missing-energy/missing-momentum measurement. For a Higgs boson at rest, the corresponding signature is quite striking, consisting of a monochromatic photon with energy $E_\gamma = m_H/2$, and similar amount of missing energy, both resonating at the Higgs mass m_H. By scrutinizing all the relevant reducible and irreducible backgrounds to the corresponding $\gamma + \not{E}_T + X$ final state, in the gluon-fusion channel, a 5σ statistical sensitivity (needed for discovery) is obtained for a branching ratio $\mathrm{BR}(H \to \gamma\bar{\gamma}) \simeq 0.1\%$ at 14 TeV, with an integrated luminosity of $L \simeq 300$ fb^{-1} [24].

The effective vertex $H\gamma\bar{\gamma}$ in Eq. (1) can be complemented by an effective $HZ\bar{\gamma}$ coupling to the Z vector boson. Both can give rise to quite distinctive new signatures at future high-energy linear and circular e^+e^- facilities (like ILC [25–27], CLIC [28], FCC-ee [29], and CEPC [30]). In particular, the $e^+e^- \to H\bar{\gamma}$ associated production of a Higgs boson and a massless dark photon via a γ/Z exchange in the s channel has been analyzed in a model-independent way at $\sqrt{s} \simeq 240$ GeV in [21]. The corresponding signature consists of a Higgs boson system (with the Higgs mainly decaying into a $b\bar{b}$ pair) recoiling against a *massless* invisible system, which remarkably has no irreducible SM background.

In this paper, we consider a different e^+e^- channel involving the $H\gamma\bar{\gamma}$ coupling. We study the $e^+e^- \to HZ$ associated production (which provides the largest Higgs-boson sample), with final states corresponding to the $H \to \gamma\bar{\gamma}$ decay. In particular, we will analyze both the leptonic $Z \to \mu^+\mu^-$ and the hadronic $Z \to q\bar{q}$ decay for the Z-boson, giving rise, respectively, to the processes

$$e^+e^- \to ZH \to \mu^+\mu^-\gamma\bar{\gamma}$$

and

$$e^+e^- \to ZH \to q\bar{q}\gamma\bar{\gamma}$$

(depicted in Fig. 1), where, as anticipated, $\bar{\gamma}$ is a massless and invisible particle.

The $\bar{\gamma}$ production mediated by a Higgs boson in e^+e^- collisions can provide complementary information to the $e^+e^- \to H\bar{\gamma}$ channel. Just as in the optimization of the $e^+e^- \to H\bar{\gamma}$ channel, requiring an invisible system with vanishing missing mass in the final state will greatly help in discriminating the $e^+e^- \to ZH \to Z\gamma\bar{\gamma}$ signal from its backgrounds. Comparison with the corresponding $\mathrm{BR}(H \to \gamma\bar{\gamma})$ experimental sensitivities from the study of the $e^+e^- \to H\bar{\gamma}$ channel and from Higgs production at the LHC will be provided, too.

In the following we will start by describing a few features of a particular theoretical framework that can indeed foresee the new decay channel $H \to \gamma\bar{\gamma}$. On the other hand, we stress that the results of the present study will actually be model independent. Indeed, the phenomenological analysis that will be described will depend on just one new beyond-the-standard-model (BSM) parameter, that is $\mathrm{BR}(H \to \gamma\bar{\gamma})$ (assuming that possible BSM deviations of other SM couplings entering the amplitude $e^+e^- \to ZH$ are subdominant).

The paper is organized as follows. In Sec. II we introduce the effective dark-photon couplings to the Higgs boson, and show some relevant model-independent parametrization of the Higgs decay BRs that are affected by the effective couplings. In Sec. III we present the phenomenological analysis of the process $e^+e^- \to ZH \to Z\gamma\bar{\gamma}$, we study how to discriminate the signal and different backgrounds for the two final states corresponding to $Z \to \mu^+\mu^-$ and $Z \to q\bar{q}$, and present the corresponding sensitivities in the $\mathrm{BR}(H \to \gamma\bar{\gamma})$ measurement. Concluding remarks are given in Sec. IV.

II. THEORETICAL FRAMEWORK

Here we present the relevant gauge-invariant dark-photon effective couplings to the Higgs boson. Although

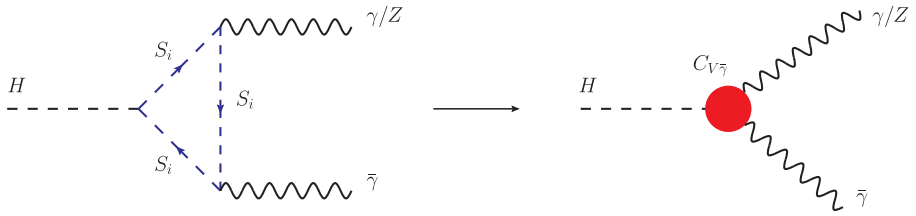

FIG. 2. Effective coupling approximation for the vertices $H\gamma\bar{\gamma}$ and $HZ\bar{\gamma}$, where S_i are the messenger fields, and in, $C_{V\bar{\gamma}}$, $V = \gamma, Z$.

these couplings will be parametrized in a model-independent way, we will use the GRFM scenario in [15] as a benchmark model which can give rise to these effective interactions.

In the GRFM framework, new effective couplings between the Higgs, photon and dark photon can be induced at one loop due to the exchange of heavy messenger fields that are charged under both the SM and the hidden $U(1)$ gauge groups (Fig. 2). The effective theory approximation can indeed be applied if the messenger sector is much heavier than both the Higgs mass m_H and the dark-fermion masses, as occurs in the GRFM, where the condition is automatically satisfied once vacuum stability bounds and dark-matter constraints are applied. In general, the NP sector will also contribute to the Higgs effective interactions with two photons, one photon and a Z, and two gluons. In the following, we do not consider the latter effects. We anyhow stress that our approach has a more general validity, being applicable to any NP scenario in which there is a heavy messenger sector that couples to both the SM fields and the $U(1)$ dark gauge sector.

In order to provide the formalism for the model-independent analysis, we give below the relevant low-energy effective Lagrangian $\mathcal{L}_{\mathrm{DP_H}}$, connecting the Higgs boson to the dark photon, that can be expressed in terms of dimensionless (real) coefficients C_{ik} (with $i, k = \bar{\gamma}, \gamma, Z$) as

$$\mathcal{L}_{\mathrm{DP_H}} = \frac{\alpha}{\pi}\left(\frac{C_{\gamma\bar{\gamma}}}{v}\gamma^{\mu\nu}\bar{\gamma}_{\mu\nu}H + \frac{C_{Z\bar{\gamma}}}{v}Z^{\mu\nu}\bar{\gamma}_{\mu\nu}H + \frac{C_{\bar{\gamma}\bar{\gamma}}}{v}\bar{\gamma}^{\mu\nu}\bar{\gamma}_{\mu\nu}H\right), \tag{3}$$

where α is the SM fine structure constant; v the SM Higgs vacuum expectation value; and $\gamma_{\mu\nu}$, $Z_{\mu\nu}$, $\bar{\gamma}_{\mu\nu}$ are the field strengths of the photon, Z boson, and dark photon, respectively ($\gamma_{\mu\nu} \equiv \partial_\mu A_\nu - \partial_\nu A_\mu$ for the photon field A_μ).

Following the usual approach, the C_{ik} coefficients in Eq. (3) can be computed in the complete theory by evaluating one-loop amplitudes for specific physical processes, and by matching them with the corresponding results obtained at tree level via the effective Lagrangian in Eq. (3). The full set of predictions for the C_{ik} coefficients for the GRFM model can be found in [21,23].

The basic C_{ik} coefficients in Eq. (3) can be directly connected to the corresponding Higgs $H \to ik$ decay widths. In particular, for the decay width $\Gamma(H \to \gamma\bar{\gamma})$, taking into account the parametrization in Eq. (3), one has [23]

$$\Gamma(H \to \gamma\bar{\gamma}) = \frac{m_H^3\alpha^2|C_{\gamma\bar{\gamma}}|^2}{8\pi^3 v^2}. \tag{4}$$

Analogous results can be obtained for the $H \to \bar{\gamma}\bar{\gamma}$ and $H \to Z\bar{\gamma}$ widths by replacing $|C_{\gamma\bar{\gamma}}|^2$ with $2|C_{\bar{\gamma}\bar{\gamma}}|^2$ and $|C_{Z\bar{\gamma}}|^2$, respectively.

In Fig. 3 we show the branching ratio for $H \to \gamma\bar{\gamma}$ in percent as a function of the corresponding $C_{\gamma\bar{\gamma}}$ coefficient (when all other effective couplings vanish). The $C_{\gamma\bar{\gamma}}$ range shown in the plot covers values naturally foreseen in the GRFM model. One can then get for the Higgs decays into a dark photon an enhancement factor $\mathcal{O}(10)$ with respect to the SM Higgs decays where the dark photon is replaced by a photon. This makes the corresponding phenomenology quite relevant for both LHC and future-collider studies.

Neglecting the $C_{Z\bar{\gamma}}$ contribution, a convenient model-independent $\mathrm{BR}(H \to \gamma\bar{\gamma}, \bar{\gamma}\bar{\gamma}, \gamma\gamma)$ parametrization can be provided, involving the *relative* exotic contributions r_{ik} to the $H \to ik$ decay widths, with $i, k = \gamma, \bar{\gamma}$, where the r_{ik} ratios are defined as

$$r_{ik} \equiv \frac{\Gamma_{ik}^{\mathrm{NP}}}{\Gamma_{\gamma\gamma}^{\mathrm{SM}}}, \tag{5}$$

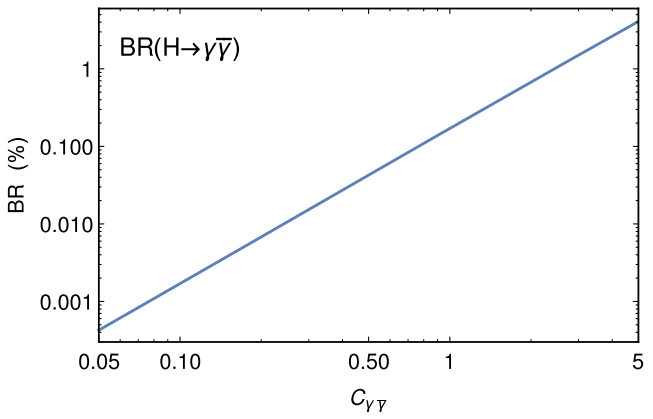

FIG. 3. Branching ratio for $H \to \gamma\bar{\gamma}$ in percent as a function of the effective coupling $C_{\gamma\bar{\gamma}}$, for all other effective couplings at their SM values. The $C_{\gamma\bar{\gamma}}$ range in the plot has been chosen so as to cover the typical BR ranges predicted by the GRFM (cf. Fig. 1 in [23]).

and $\Gamma_{ik}^{\rm NP}$ stands for the pure NP contribution to the $H \to ik$ decay width.[1] Then, the following model-independent parametrization of the quantities $\mathrm{BR}_{\gamma\bar{\gamma},\bar{\gamma}\bar{\gamma},\gamma\gamma} \equiv \mathrm{BR}(H \to \gamma\bar{\gamma}, \bar{\gamma}\bar{\gamma}, \gamma\gamma)$ as functions of r_{ik} holds [23],

$$
\begin{aligned}
BR_{\gamma\bar{\gamma}} &= BR_{\gamma\gamma}^{\rm SM} \frac{r_{\gamma\bar{\gamma}}}{1 + r_{\bar{\gamma}\bar{\gamma}} BR_{\gamma\gamma}^{\rm SM}}, \\
BR_{\bar{\gamma}\bar{\gamma}} &= BR_{\gamma\gamma}^{\rm SM} \frac{r_{\bar{\gamma}\bar{\gamma}}}{1 + r_{\bar{\gamma}\bar{\gamma}} BR_{\gamma\gamma}^{\rm SM}}, \\
BR_{\gamma\gamma} &= BR_{\gamma\gamma}^{\rm SM} \frac{(1 + \chi\sqrt{r_{\gamma\gamma}})^2}{1 + r_{\bar{\gamma}\bar{\gamma}} BR_{\gamma\gamma}^{\rm SM}},
\end{aligned}
\tag{6}
$$

where $\chi = \pm 1$ parametrizes the relative sign between the SM and the NP loop amplitudes.

We stress that, in any model where the effective couplings in Eq. (3) are generated radiatively by charged messenger fields circulating in the loop, the factors r_{ik} (where $i, k = \gamma, \bar{\gamma}, Z$) are not independent, but are determined by the hypercharge assignment of the mediators, as described in [21].

A consequence of Eq. (6) is that these scenarios can also be indirectly constrained by a precision measurement of the Higgs branching ratios for the more-standard decays into two photons or invisible final states.

III. COLLIDER ANALYSIS

In this section we discuss the experimental strategies relevant to make a measurement of $\mathrm{BR}_{\gamma\bar{\gamma}}$, the Higgs decay BR into a photon and an invisible massless dark photon, via the process $e^+e^- \to ZH$ followed by $H \to \gamma\bar{\gamma}$ in an e^+e^- collider with c.m. energy of about 240 GeV, which maximizes the Higgs cross section. This setup could be realized at either linear (like ILC) or circular (like FCC-ee and CEPC) facilities with integrated luminosities up to about 10 ab^{-1} at 240 GeV, corresponding to the production of up to about 2 million Higgs bosons.

We outline the search strategies for both the leptonic $Z \to \ell^+\ell^-$ and hadronic $Z \to q\bar{q}$ final states (cf. Fig. 1). Being stable and escaping the detection, a massless dark photon shows up in normal detectors like a neutrino. Thus the $e^+e^- \to ZH$ leptonic final state consists of a pair of opposite-sign same-flavor leptons, a photon, and missing energy/momentum (named $\not{E}/\not{p}$), whereas the hadronic final state contains two jets, a photon, and missing energy/momentum.

We have simulated the signal and SM backgrounds with MadGraph5_aMC@NLO[31] interfaced with PYTHIA [32] to include the initial- and final-state radiation and hadronization effects.[2] The jets are clustered using a simple cone algorithm with cone size $R = 0.4$ and transverse momentum $p_T > 20$ GeV.

We assume the following specification for the detector performance [33,34]:

(i) Muon momentum resolution: $\Delta p/p = 0.1\% + p_T/(10^5\ \mathrm{GeV})$ for $|\eta| < 1$, and 10 times poorer for $1 < |\eta| < 2.5$.
(ii) Photon energy resolution: $\Delta E/E = 16.6\%/\sqrt{E/\mathrm{GeV}} + 1.1\%$.
(iii) Jet energy resolution: $\Delta E/E = 30\%/\sqrt{E/\mathrm{GeV}}$.
(iv) Particle identification efficiency for muons and photons: 99% for $p_T > 10$ GeV.

A. Leptonic channel: $e^+e^- \to ZH \to \mu^+\mu^-\gamma\bar{\gamma}$

Thanks to the superior momentum resolution, the leptonic channel is the cleanest of the final states, as the leptonic Z can be reconstructed very efficiently. Since the muon momentum resolution is better than the one for electrons, we outline here the search for the $Z \to \mu^+\mu^-$ channel. The electron channel will contribute less to the total $e^+e^- \to ZH$ sensitivity not only for the poorer electron momentum resolution, but also for the additional SM neutral-current t-channel $e^+e^- \to e^+e^-\bar{\nu}\nu\gamma$ component in the background, which has no equivalent for the muonic final state. Initially, we select the events containing two opposite-sign muons and a single photon with the following *basic cuts*:

(i) muon and photon transverse momentum with $p_T^\mu, p_T^\gamma > 10$ GeV,
(ii) muon and photon pseudorapidity in the range $|\eta^\mu|, |\eta^\gamma| < 2.5$,
(iii) missing energy with $\not{E} > 10$ GeV,
(iv) angular separation between any two objects with $\Delta R > 0.2$,
(v) jet veto for $p_T^j > 20$ GeV.

The irreducible SM background for the $e^+e^- \to ZH \to \mu^+\mu^-\gamma\bar{\gamma}$ final state is given by the process $e^+e^- \to \mu^+\mu^-\nu\bar{\nu}\gamma$, which arises from the resonant contribution of the channels $e^+e^- \to ZZ\gamma$ and $e^+e^- \to WW\gamma$, as well as from different t-channel processes such as $e^+e^- \to \nu\bar{\nu}Z\gamma$. In the analysis of the irreducible $\mu^+\mu^-\nu\bar{\nu}\gamma$ background both the individual resonant $WW\gamma$ and $ZZ\gamma$ components will be analyzed in parallel to the inclusive $\mu^+\mu^-\nu\bar{\nu}\gamma$ production. Then, there are reducible backgrounds from $Z\gamma$ events accompanied by fake missing energy, which can originate from initial-state radiation/beamstrahlung, mismeasurement of the lepton or photon momenta, or missed final-state objects. The last category contains the $e^+e^- \to ZH \to \mu^+\mu^-\gamma\gamma$ process when one of the photons escapes detection. The latter events will have

[1] Note that in the case of $\Gamma_{\gamma\gamma}^{\rm NP}$, this quantity is connected to a physical decay width only up to possible interference terms between the SM and the NP $H \to \gamma\gamma$ amplitudes.

[2] Initial-state radiation effects considered here will be typical of circular e^+e^- colliders, as we will disregard possible beamstrahlung effects.

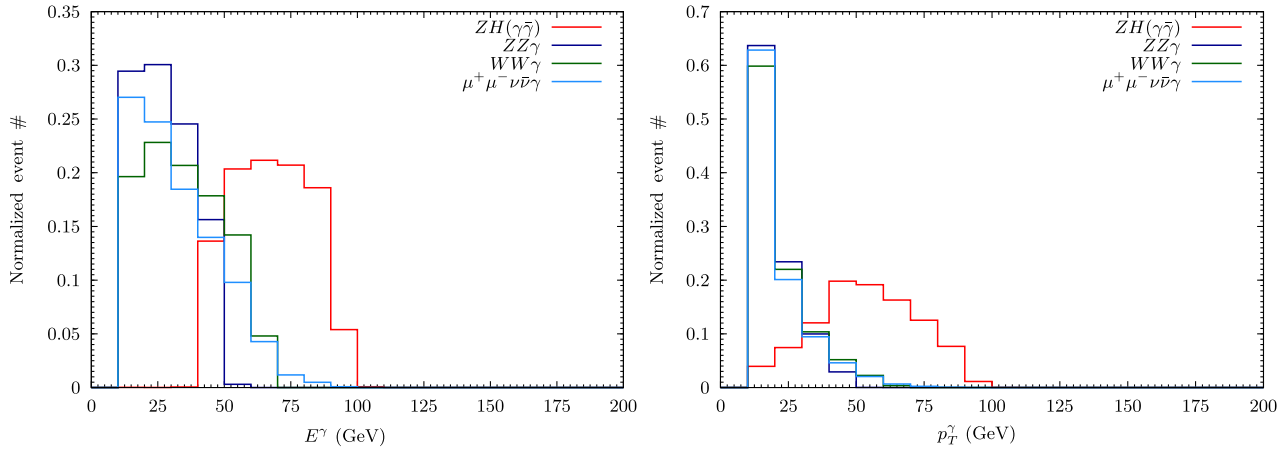

FIG. 4. The photon energy and transverse momentum distributions for the $e^+e^- \to \mu^+\mu^-\gamma\bar{\gamma}$ signal and $e^+e^- \to \mu^+\mu^-\nu\bar{\nu}\gamma$ background, after applying the set of basic cuts, at $\sqrt{s} = 240$ GeV. Results for the individual resonant $WW\gamma$ and $ZZ\gamma$ background components are also shown.

the same kinematic features as the signal, but the rates are suppressed by both $\mathrm{BR}(H \to \gamma\gamma) \simeq 2 \times 10^{-3}$ and the small probability of missing one of the photons while the other goes inside the central barrel and passes the event selection. Further details will follow on the (in general negligible) $H \to \gamma\gamma$ contribution to the background.[3]

The photon energy and transverse momentum normalized distributions are shown in Fig. 4 both for signal and main backgrounds, after implementing the above list of basic cuts.

Apart from the latter distributions, signal events can be particularly discriminated by the use of a few kinematic variables characterizing them. Three variables are of special interest: the missing mass M_{miss}, the invariant mass of the photon-missing-energy system $M_{\gamma\bar{\gamma}}$, and the invariant mass of the lepton pair $M_{\ell\ell}$. These are defined as

$$M_{\mathrm{miss}} = \sqrt{\not{E}^2 - \vec{\not{p}}^2}, \tag{7}$$

$$M_{\gamma\bar{\gamma}} = \sqrt{2(E_\gamma \not{E} - \vec{p}_\gamma \cdot \vec{\not{p}})}, \tag{8}$$

$$M_{\ell\ell} = \sqrt{2(E_{\ell^+}E_{\ell^-} - \vec{p}_{\ell^+} \cdot \vec{p}_{\ell^-})}, \tag{9}$$

where the missing energy $\not{E}$ and momentum $\vec{\not{p}}$ are experimentally defined by the equations $\not{E} = \sqrt{s} - \sum_i E_i$ and $\vec{\not{p}} = -\sum_i \vec{p}_i$ (the sum is over all detected final particles). For the signal events, where the missing energy is carried by the massless dark photon, these variables are centered at $M_{\mathrm{miss}} = 0$, $M_{\gamma\bar{\gamma}} = m_H$ and $M_{\ell\ell} = M_Z$.

[3]We have also scrutinized the nonresonant $e^+e^- \to \mu^+\mu^-\gamma\gamma$ channel, and found that in general this background can be controlled by demanding an extra missing transverse-energy lower cut of a few GeV over the final cut flow, without affecting our present analysis.

The $M_{\mu^+\mu^-}$ and $M_{\gamma\bar{\gamma}}$ normalized distributions for the signal and SM-background events are shown in Fig. 5. The $M_{\mu^+\mu^-}$ distribution is obtained assuming the basic cuts listed above. An additional cut 86 GeV $< M_{\mu^+\mu^-} <$ 96 GeV has been applied before plotting the $M_{\gamma\bar{\gamma}}$ distribution.

We therefore suppress the SM background by the following selection criteria imposed on top of the basic cuts:

(i) Z mass cut: 86 GeV $< M_{\mu^+\mu^-} <$ 96 GeV,

(ii) Higgs mass cut: 120 GeV $< M_{\gamma\bar{\gamma}} <$ 130 GeV.

After applying the above two cuts, one obtains the M_{miss} and $\not{E}$ normalized distributions shown in Fig. 6. Because of the signal low-mass structure in the M_{miss} distribution in Fig. 6, we then impose the additional cut

(iii) Missing mass cut: $M_{\mathrm{miss}} < 20$ GeV.

Cutting away large M_{miss} values proves indeed very effective for background suppression, since most of the background subprocesses contain massive invisible systems which are not likely to have low M_{miss}.

We then stop our cut flow, since, after applying the M_{miss} optimization on distributions in Fig. 6, the $\not{E}$ distribution (that is largely correlated to the M_{miss} distribution) does not offer an extra handle for further optimization.

We now comment on the reducible SM contribution to the background coming from $e^+e^- \to ZH \to \mu^+\mu^-\gamma\gamma$, where one of the photons in the $H \to \gamma\gamma$ decay is not identified. Indeed, some $\not{E}$ can come from either energy mismeasurement or the unlikely situation where just one of the photons lies in the forward region ($|\eta| > 5$) and is not detected, or a combination of both. For $BR_{\gamma\bar{\gamma}} = 1\%$, we checked that the $ZH \to Z\gamma\gamma$ background is suppressed by two orders of magnitude with respect to the signal (by imposing the cut flow in Table I). For $BR_{\gamma\bar{\gamma}} \simeq BR_{\gamma\gamma}$, the

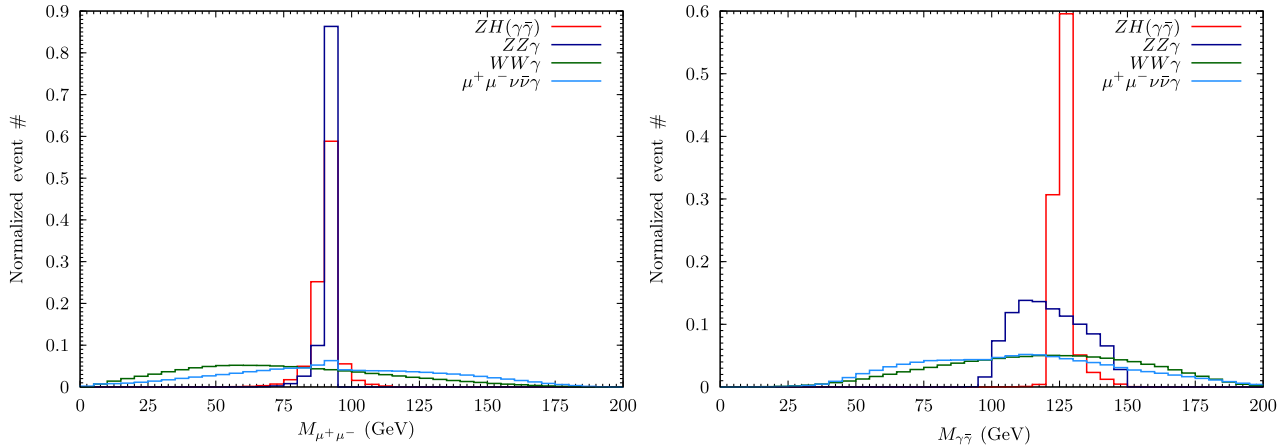

FIG. 5. The $\mu^+\mu^-$ and $\gamma\bar{\gamma}$ invariant-mass distributions for the $e^+e^- \to \mu^+\mu^-\gamma\bar{\gamma}$ signal and $e^+e^- \to \mu^+\mu^-\nu\bar{\nu}\gamma$ background, for $\sqrt{s} = 240$ GeV. The $M_{\mu^+\mu^-}$ distributions are obtained after imposing just the set of basic cuts described in the text, whereas the $M_{\gamma\bar{\gamma}}$ distribution is affected by an additional cut 86 GeV $< M_{\mu^+\mu^-} <$ 96 GeV. Results for the individual resonant $WW\gamma$ and $ZZ\gamma$ background components are also shown.

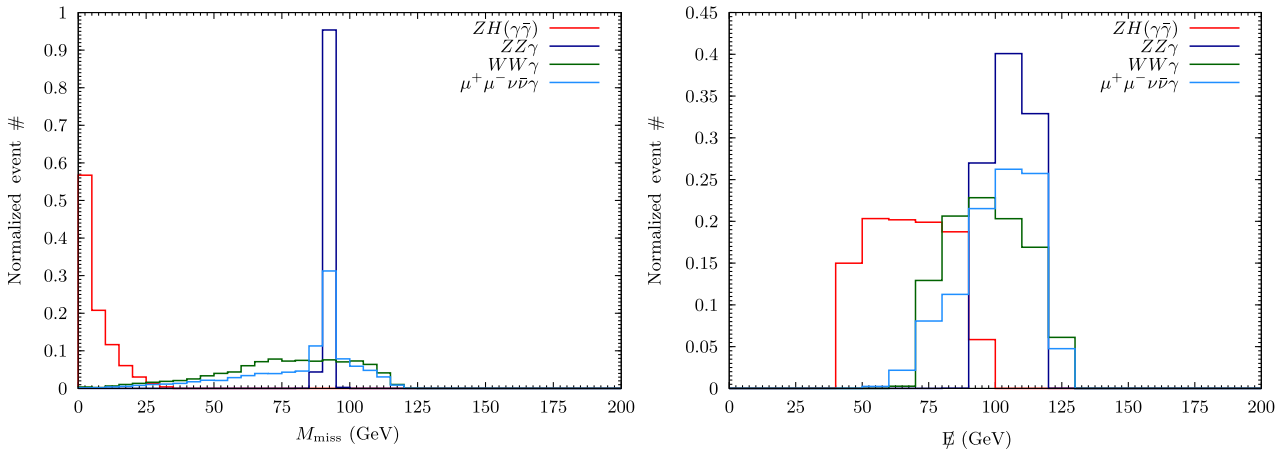

FIG. 6. The missing-mass and missing-energy distributions for the $e^+e^- \to \mu^+\mu^-\gamma\bar{\gamma}$ signal and $e^+e^- \to \mu^+\mu^-\nu\bar{\nu}\gamma$ background, for $\sqrt{s} = 240$ GeV, after imposing the invariant-mass cuts around the M_Z and m_H on the $\mu^+\mu^-$ and $\gamma\bar{\gamma}$ systems, respectively.

number of signal events is still about 30 times the number of these background events.

The effect of these cuts on the signal and inclusive background event yields is presented in Table I. The resulting significance $S/\sqrt{S+B}$ (where S is the number of signal events and B the number of background events) is shown as a function of $BR_{\gamma\bar{\gamma}}$ in Fig. 7, assuming an integrated luminosity of 10 ab^{-1} at $\sqrt{s} = 240$ GeV. We find that in the leptonic channel one can exclude values down to $BR_{\gamma\bar{\gamma}} = 2 \times 10^{-4}$ at 95% C.L., while the 5σ discovery reach is $BR_{\gamma\bar{\gamma}} = 7.5 \times 10^{-4}$.

TABLE I. Event yields after sequential cuts for $e^+e^- \to ZH \to \mu^+\mu^-\gamma\bar{\gamma}$ and corresponding background, for an integrated luminosity of 10 ab^{-1}, and c.m. energy $\sqrt{s} = 240$ GeV. The signal yield has been normalized assuming $BR_{\gamma\bar{\gamma}} = 0.1\%$.

Process	Basic cuts	$M_{\ell\ell}$ cut	$M_{\gamma\bar{\gamma}}$ cut	$M_{\rm miss}$ cut
$\mu^+\mu^-\gamma\bar{\gamma}$ ($BR_{\gamma\bar{\gamma}}$=0.1%)	65.3	54.9	49.7	47.3
$\mu^+\mu^-\nu\bar{\nu}\gamma$	5.00×10^4	5.73×10^3	1.09×10^3	15

B. Hadronic channel: $e^+e^- \to ZH \to q\bar{q}\gamma\bar{\gamma}$

The worse energy resolution for jets with respect to muons, resulting in a less clean reconstruction of the hadronic Z-boson decay, can be compensated by the larger Z branching ratio into jets, and the increased phase-space acceptance for jets. It is then important to include the Z hadronic decay mode in the present analysis.

The $e^+e^- \to ZH \to q\bar{q}\gamma\bar{\gamma}$ signal consists of two jets, a single photon, and missing energy. The main irreducible SM background comes from the process $e^+e^- \to q\bar{q}\nu\bar{\nu}\gamma$, which, as we will show in the following, can be effectively suppressed by imposing an upper missing-mass cut. The main reducible and dominant background arises instead

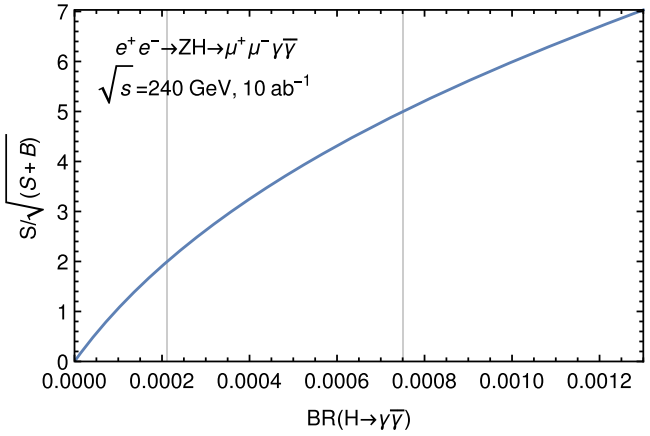

FIG. 7. Signal significance for the $e^+e^- \to ZH \to \mu^+\mu^-\gamma\bar{\gamma}$ channel versus $BR_{\gamma\bar{\gamma}}$ for 10 ab^{-1} at 240 GeV. The left vertical grey line corresponds to a 95% C.L. exclusion, while the right line points to the 5σ discovery reach.

from the jet-pair production accompanied by a hard photon, $e^+e^- \to q\bar{q}\gamma \to jj\gamma$. Here, some missing energy is generated either from jet-energy mismeasurement or, more importantly, by neutrinos generated by heavy-flavor decays inside the jet showering. The $jj\gamma$ background is then characterized by relatively low values of missing energy and by the approximate alignment of the missing momentum with one of the jets.

We perform the initial event selection according to the following *basic cuts*:

(i) lepton veto for $p_T^\ell > 10$ GeV and $|\eta^\ell| < 2.5$,
(ii) for the photon transverse momentum and pseudorapidity, $p_T^\gamma > 10$ GeV, $|\eta^\gamma| < 2.5$,
(iii) for the jet transverse momentum and pseudorapidity, $p_T^j > 20$ GeV, $|\eta^j| < 5.0$,
(iv) for the missing energy, $\not{E} > 10$ GeV,
(v) for the angular separation between any pair of visible objects, $\Delta R > 0.4$.

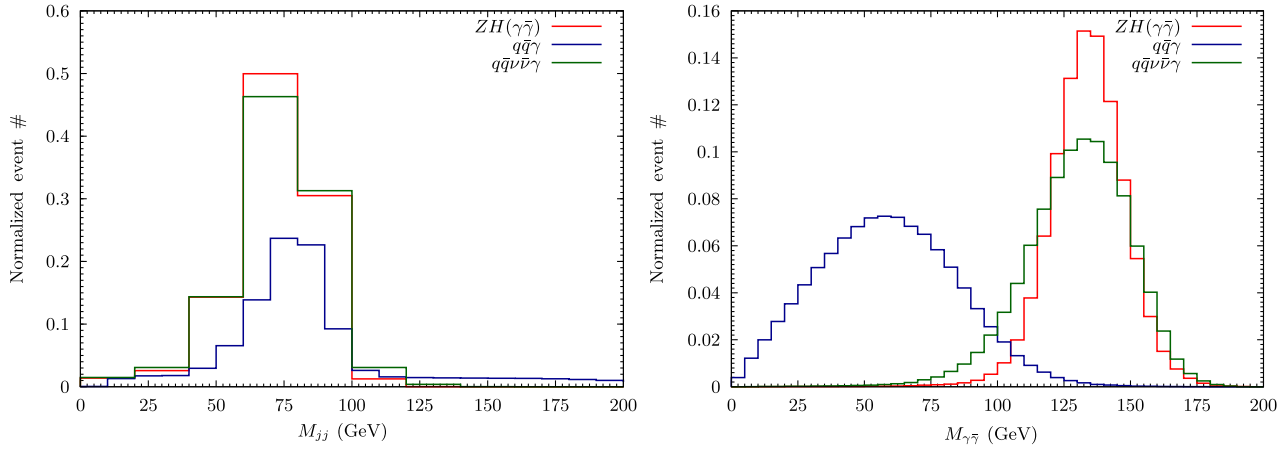

FIG. 8. The jj and $\gamma\bar{\gamma}$ invariant-mass distributions for the $e^+e^- \to ZH \to q\bar{q}\gamma\bar{\gamma}$ signal and backgrounds, for $\sqrt{s} = 240$ GeV. The M_{jj} distribution is obtained after imposing the set of basic cuts described in the text, whereas the $M_{\gamma\bar{\gamma}}$ distribution is obtained with an additional 50 GeV $< M_{jj} <$ 90 GeV cut.

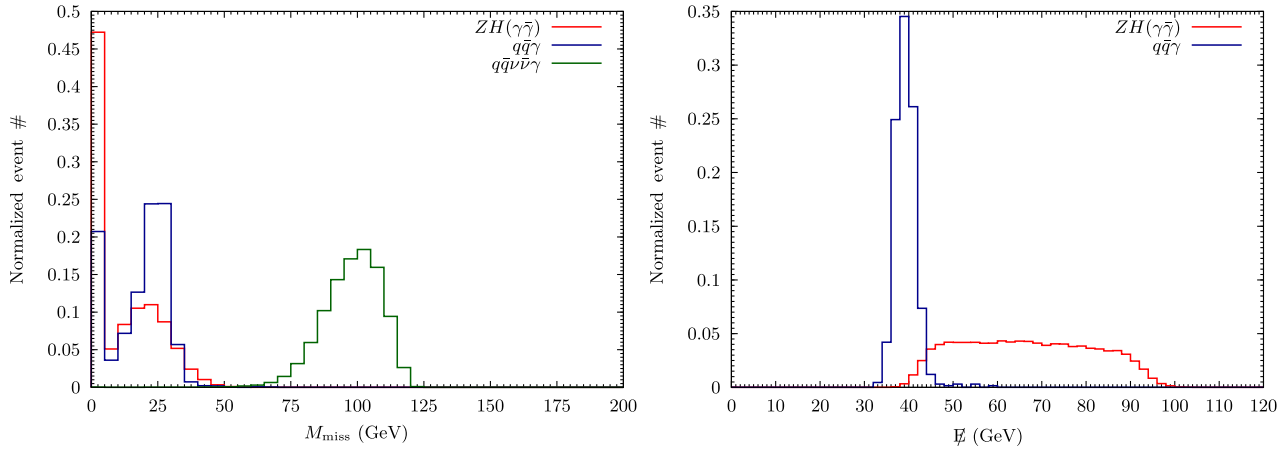

FIG. 9. The missing mass and missing energy distributions for the $e^+e^- \to ZH \to q\bar{q}\gamma\bar{\gamma}$ signal and corresponding backgrounds, for $\sqrt{s} = 240$ GeV. The $M_{\rm miss}$ distribution is obtained after imposing invariant-mass cuts on the jj and $\gamma\bar{\gamma}$ systems around M_Z and m_H, respectively, as described in the text. In the $\not{E}$ distributions, an additional $M_{\rm miss} < 20$ GeV cut is imposed.

TABLE II. Event yields after sequential cuts described in the text for $e^+e^- \to ZH \to q\bar{q}\gamma\bar{\gamma}$, and corresponding backgrounds, for an integrated luminosity of 10 ab^{-1}, and c.m. energy $\sqrt{s} = 240$ GeV. The signal yield has been normalized assuming $BR_{\gamma\bar{\gamma}} = 0.1\%$. Dashes stand for event yields less than 1.

Process	Basic cuts	M_{jj} cut	$M_{\gamma\bar{\gamma}}$ cut	$M_{\rm miss}$ cut	$\not{E}$ cut
$jj\gamma\bar{\gamma}$ ($BR_{\gamma\bar{\gamma}} = 0.1\%$)	804	669	154	110	72
$jj\gamma$	3.39×10^7	2.26×10^7	1.47×10^5	6.5×10^4	–
$jj\nu\bar{\nu}\gamma$	3.9×10^4	3.1×10^4	5.9×10^3	2.2	–

We use the same kinematical variables adopted in the lepton-channel analysis, with the obvious replacement of $M_{\ell\ell}$ with the jet-pair invariant mass M_{jj}.

Then, for the signal events, where the missing energy is carried by the massless dark photon, the relevant variables are centered at $M_{\rm miss} = 0$, $M_{\gamma\bar{\gamma}} = m_H$, and $M_{jj} = M_Z$.

The M_{jj} and $M_{\gamma\bar{\gamma}}$ normalized distributions for the signal and SM-background events are shown in Fig. 8. The M_{jj} distribution is obtained assuming the basic cuts listed above. An additional cut 50 GeV $< M_{jj} <$ 90 GeV has been applied before plotting the $M_{\gamma\bar{\gamma}}$ distribution (due to the relatively poor jet-energy resolution, the M_{jj} cut around the Z-boson mass is looser than the $M_{\mu^+\mu^-}$ cut for the leptonic channel).

In Fig. 8, one can see how the extra missing-momentum system arising from the $Z \to \bar{q}q$ showering widens up the signal $M_{\gamma\bar{\gamma}}$ peak structure around m_H with respect to the leptonic-channel $M_{\gamma\bar{\gamma}}$ distribution in Fig. 5. Nevertheless, we found that loosening the 120 GeV $< M_{\gamma\bar{\gamma}} <$ 130 GeV cut (applied in the leptonic channel) in order to increase the signal statistics induces a milder kinematical characterization of the signal events, contaminating them with extra missing energy not originating from the dark photon. This in turn would make further cuts on the $M_{\rm miss}$ less effective for separating the signal from the $q\bar{q}\gamma$ background.

As a consequence, we stick to the *narrow* 120 GeV $< M_{\gamma\bar{\gamma}} <$ 130 GeV cut, hence selecting signal events where the missing momentum is mostly associated to the dark photon. This is anyhow very effective in reducing the $q\bar{q}\gamma$ background (cf. Fig. 8). After that, one obtains the $M_{\rm miss}$ normalized distribution shown in Fig. 9 (left plot). Hence, requiring $M_{\rm miss} < 20$ GeV effectively kills the irreducible $q\bar{q}\nu\bar{\nu}\gamma$ background, with a more moderate effect on the $q\bar{q}\gamma$ reducible component.

In Fig. 9 (right plot), we have imposed an additional $M_{\rm miss} < 20$ GeV cut on the normalized $\not{E}$ distribution. In order to further mitigate the remaining $q\bar{q}\gamma$ background, one can cut away the region $\not{E} \lesssim 50$ GeV. We then add a further optimized missing-energy cut $\not{E} > 59$ GeV to the cut flow. After that also the $q\bar{q}\gamma$ background is reduced to a negligible level, and the search, assuming a reference decay rate $BR_{\gamma\bar{\gamma}} = 0.1\%$, becomes essentially a counting experiment for the signal events.

The effect of the cut flow on the event yields for the signal (for $BR_{\gamma\bar{\gamma}} = 0.1\%$) and backgrounds is shown in Table II, assuming an integrated luminosity of 10 ab^{-1}. In Fig. 10, the resulting significance is shown as a function of

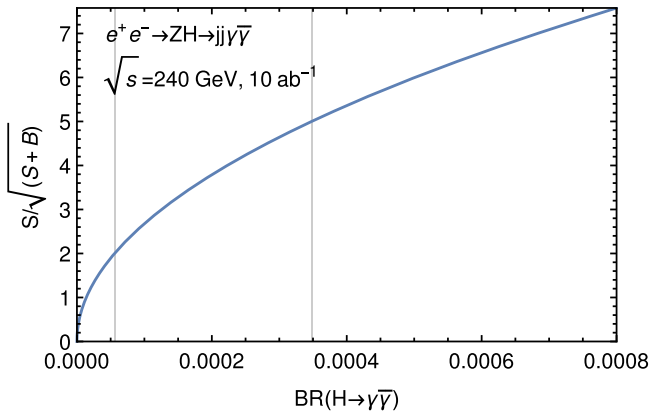

FIG. 10. Signal significance for the $e^+e^- \to ZH \to q\bar{q}\gamma\bar{\gamma}$ channel versus $BR_{\gamma\bar{\gamma}}$ for 10 ab^{-1} at 240 GeV. The left vertical grey line corresponds to a 95% C.L. exclusion, while the right line points to the 5σ discovery reach.

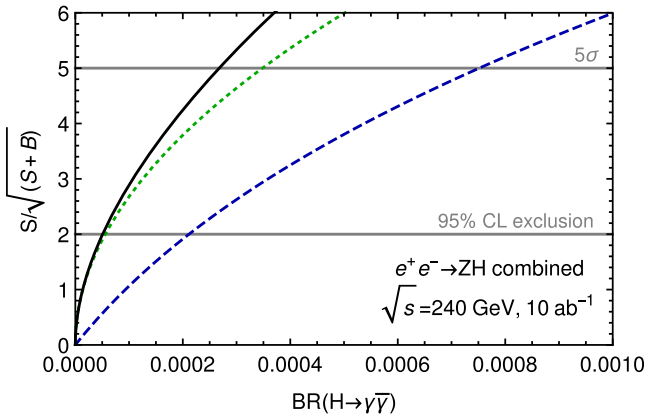

FIG. 11. Signal significance in the $e^+e^- \to ZH \to q\bar{q}\gamma\bar{\gamma}$ channel (green dotted line), $e^+e^- \to ZH \to \mu^+\mu^-\gamma\bar{\gamma}$ channel (blue dashed line) and in the combined search (black solid line) versus $BR_{\gamma\bar{\gamma}}$ for 10 ab^{-1} at $\sqrt{s} = 240$ GeV. The lower and upper horizontal lines pinpoint, respectively, the 95% C.L. exclusion bound, and the 5σ-significance discovery reach.

$BR_{\gamma\bar{\gamma}}$. We find a considerably better sensitivity compared to the muon channel, with the 5σ discovery reach extending down to $BR_{\gamma\bar{\gamma}} \simeq 3.5 \times 10^{-4}$ (i.e., roughly a factor 2 better than in the leptonic channel), and exclusion at 95% C.L. for $BR_{\gamma\bar{\gamma}} \simeq 0.5 \times 10^{-4}$ (i.e., about a factor 4 better than in the leptonic channel).

Finally, in Fig. 11, we present the combined significance for the leptonic and hadronic searches. The combined 5σ sensitivity for discovery reaches $BR_{\gamma\bar{\gamma}} \simeq 2.7 \times 10^{-4}$, while the 95% C.L. exclusion reach is dominated by the hadronic channel sensitivity, and is again $BR_{\gamma\bar{\gamma}} \simeq 0.5 \times 10^{-4}$.

IV. CONCLUSIONS

A class of models potentially explaining the observed fermion mass hierarchy may naturally predict the decay of the Higgs boson into a photon and a dark photon $\bar{\gamma}$ which is massless and undetectable by collider experiments. Thanks to the nondecoupling properties of the Higgs boson, the corresponding branching ratio can be up to a few percent.

We have studied the potential of high-energy e^+e^- facilities to either discover the $H \to \gamma\bar{\gamma}$ decay or constrain its branching ratio. In particular, we have analyzed the process $e^+e^- \to HZ$ followed by $H \to \gamma\bar{\gamma}$, considering both the leptonic channel where $Z \to \mu^+\mu^-$ and the hadronic channel where $Z \to q\bar{q}$, in e^+e^- collisions with integrated luminosity 10 ab^{-1} at $\sqrt{s} \simeq 240$ GeV. In this setup, the production of about 2 million Higgs bosons is foreseen. We included initial-state radiation effects typical of a circular collider, shower effects for the jet final states, and detector resolutions as presently foreseen for ILC detectors.

We find that both the leptonic and hadronic Z decay modes considerably contribute to the $e^+e^- \to ZH$ sensitivity, with a quite higher potential for the hadronic mode. We have not analyzed the $Z \to e^+e^-$ mode, which is expected to suffer from larger backgrounds and worse detector resolution with respect to $Z \to \mu^+\mu^-$.

Discovery of the $H \to \gamma\bar{\gamma}$ decay with a 5σ sensitivity is reached in $e^+e^- \to ZH$ for a branching ratio $BR_{\gamma\bar{\gamma}} \approx 2.7 \times 10^{-4}$ by combining both muon and hadronic channels, while the corresponding 95% C.L. exclusion reach is at $BR_{\gamma\bar{\gamma}} \simeq 0.5 \times 10^{-4}$.

Note that this exclusion reach is more than two orders of magnitude better than the corresponding reach of the process $e^+e^- \to H\bar{\gamma}$ analyzed in [21]. On the other hand, the $e^+e^- \to ZH$ 5σ discovery reach is more than three times better than the LHC reach with 300 fb^{-1}, and comparable to the HL-LHC expected sensitivity, according to the preliminary analysis in [24]. Hence, the $e^+e^- \to ZH$ channel at FCC-ee/CEPC provides a particularly sensitive probe to the Higgs branching ratio into a photon plus dark photon.

We stress that this analysis is model independent, and its results can be universally applied to the search for any Higgs two-body decay into a photon plus an undetected light particle, under the assumption of a SM $e^+e^- \to ZH$ cross section. A modified Higgs production cross section can anyway be independently rescaled from our results.

Before concluding we note that the present analysis does not include *machine-induced* backgrounds. In particular, beamstrahlung can considerably affect the impact of selection cuts in our signal-over-background optimization strategy, by broadening the collision c.m. energy distribution. On the other hand, beamstrahlung is very much dependent on the actual accelerator technology, and circular machines are much less affected by beamstrahlung with respect to linear colliders. In fact, this potentially relevant effect can be accurately described only after the basic machine parameters (and a particular scheme for beam bunches) will be set up (see for instance [35]). We anyhow think that the inclusion of such machine-induced backgrounds is beyond the scope of the present study.

ACKNOWLEDGMENTS

E. G. would like to thank the CERN Theoretical Physics Department for its kind hospitality during the preparation of this work. The work of M. H. has been supported by the Academy of Finland, Grant No. 267842.

[1] G. Aad *et al.* (ATLAS Collaboration), Observation of a new particle in the search for the Standard Model Higgs boson with the ATLAS detector at the LHC, Phys. Lett. B **716**, 1 (2012); S. Chatrchyan *et al.* (CMS Collaboration), Observation of a new boson at a mass of 125 GeV with the CMS experiment at the LHC, Phys. Lett. B **716**, 30 (2012).

[2] F. Englert and R. Brout, Broken Symmetry and the Mass of Gauge Vector Mesons, Phys. Rev. Lett. **13**, 321 (1964); P. W. Higgs, Broken symmetries, massless particles and gauge fields, Phys. Lett. **12**, 132 (1964); P. W. Higgs, Broken Symmetries and the Masses of Gauge Bosons, Phys. Rev. Lett. **13**, 508 (1964); G. S. Guralnik, C. R. Hagen, and T. W. B. Kibble, Global Conservation Laws and Massless Particles, Phys. Rev. Lett. **13**, 585 (1964).

[3] G. Aad *et al.* (ATLAS and CMS Collaborations), Measurements of the Higgs boson production and decay rates and constraints on its couplings from a combined ATLAS and

CMS analysis of the LHC pp collision data at $\sqrt{s} = 7$ and 8 TeV, J. High Energy Phys. 08 (2016) 045.

[4] P. A. R. Ade *et al.* (Planck Collaboration), Planck 2013 results. XVI. Cosmological parameters, Astron. Astrophys. **571**, A16 (2014).

[5] P. A. R. Ade *et al.* (Planck Collaboration), Planck 2015 results. XIII. Cosmological parameters, Astron. Astrophys. **594**, A13 (2016).

[6] L. Ackerman, M. R. Buckley, S. M. Carroll, and M. Kamionkowski, Dark matter and dark radiation, Phys. Rev. D **79**, 023519 (2009).

[7] N. Arkani-Hamed, D. P. Finkbeiner, T. R. Slatyer, and N. Weiner, A theory of dark matter, Phys. Rev. D **79**, 015014 (2009).

[8] J. Fan, A. Katz, L. Randall, and M. Reece, Dark-Disk Universe, Phys. Rev. Lett. **110**, 211302 (2013).

[9] M. Heikinheimo, M. Raidal, C. Spethmann, and H. Veermäe, Dark matter self-interactions via collisionless shocks in cluster mergers, Phys. Lett. B **749**, 236 (2015).

[10] B. Holdom, Two U(1)'s and epsilon charge shifts, Phys. Lett. **166B**, 196 (1986).

[11] S. A. Abel, M. D. Goodsell, J. Jaeckel, V. V. Khoze, and A. Ringwald, Kinetic mixing of the photon with kidden U(1)s in string phenomenology, J. High Energy Phys. 07 (2008) 124; M. Goodsell, J. Jaeckel, J. Redondo, and A. Ringwald, Naturally light hidden photons in LARGE volume string compactifications, J. High Energy Phys. 11 (2009) 027; S. Baek, P. Ko, and W. I. Park, Singlet portal extensions of the standard seesaw models to a dark sector with local dark symmetry, J. High Energy Phys. 07 (2013) 013; S. Andreas, M. D. Goodsell, and A. Ringwald, Hidden photons in connection to dark matter, AIP Conf. Proc. **1563**, 114 (2013); H. An, M. Pospelov, and J. Pradler, New light on dark photons, arXiv:1309.6599; S. Baek, P. Ko, and W. I. Park, Hidden sector monopole, vector dark matter and dark radiation with higgs portal, J. Cosmol. Astropart. Phys. 10 (2014) 067; H. Vogel and J. Redondo, Dark radiation constraints on minicharged particles in models with a hidden photon, J. Cosmol. Astropart. Phys. 02 (2014) 029; K. Petraki, L. Pearce, and A. Kusenko, Self-interacting asymmetric dark matter coupled to a light massive dark photon, J. Cosmol. Astropart. Phys. 07 (2014) 039; V. V. Khoze and G. Ro, Dark matter monopoles, vectors and photons, J. High Energy Phys. 10 (2014) 61; J. Jaeckel, S. Roy, and C. J. Wallace, Hidden photons with Kaluza-Klein towers, arXiv:1408.0019; B. Brahmachari and A. Raychaudhuri, Kinetic mixing and symmetry breaking dependent interactions of the dark photon, Nucl. Phys. **B887**, 441 (2014); P. Ko, Dark matter, dark radiation and Higgs phenomenology in the hidden sector DM models, Nucl. Part. Phys. Proc. **263–264**, 101 (2015).

[12] V. M. Abazov *et al.* (D0 Collaboration), Search for Dark Photons from Supersymmetric Hidden Valleys, Phys. Rev. Lett. **103**, 081802 (2009); S. Andreas, C. Niebuhr, and A. Ringwald, New limits on hidden photons from past electron beam dumps, Phys. Rev. D **86**, 095019 (2012); G. Agakishiev *et al.* (HADES Collaboration), Searching a Dark Photon with HADES, Phys. Lett. B **731**, 265 (2014); S. N. Gninenko, Search for MeV dark photons in a light-shining-through-walls experiment at CERN, Phys. Rev. D **89**, 075008 (2014); J. P. Lees *et al.* (*BABAR* Collaboration), Search for a Dark Photon in e^+e^- Collisions at *BABAR*, Phys. Rev. Lett. **113**, 201801 (2014); D. Curtin, R. Essig, S. Gori, and J. Shelton, Illuminating dark photons with high-energy colliders, J. High Energy Phys. 02 (2015) 157; I. Jaegle (Belle Collaboration), Search for the Dark Photon and the Dark Higgs Boson at Belle, Phys. Rev. Lett. **114**, 211801 (2015).

[13] R. Essig *et al.*, Working Group Report: New light weakly coupled particles, arXiv:1311.0029.

[14] P. Agrawal, F. Y. Cyr-Racine, L. Randall, and J. Scholtz, Make dark matter charged again, J. Cosmol. Astropart. Phys. 05 (2017) 022.

[15] E. Gabrielli and M. Raidal, Exponentially spread dynamical Yukawa couplings from nonperturbative chiral symmetry breaking in the dark sector, Phys. Rev. D **89**, 015008 (2014).

[16] B. Moore, Evidence against dissipationless dark matter from observations of galaxy haloes, Nature (London) **370**, 629 (1994).

[17] A. A. Klypin, A. V. Kravtsov, O. Valenzuela, and F. Prada, Where are the missing Galactic satellites?, Astrophys. J. **522**, 82 (1999).

[18] D. N. Spergel and P. J. Steinhardt, Observational Evidence for Self-Interacting Cold Dark Matter, Phys. Rev. Lett. **84**, 3760 (2000).

[19] H. E. Haber and G. L. Kane, The search for supersymmetry: Probing physics beyond the Standard Model, Phys. Rep. **117**, 75 (1985).

[20] E. Gabrielli, L. Marzola, and M. Raidal, Radiative yukawa couplings in the simplest left-right symmetric model, Phys. Rev. D **95**, 035005 (2017).

[21] S. Biswas, E. Gabrielli, M. Heikinheimo, and B. Mele, Higgs-boson production in association with a dark photon in $e^+e^?$ collisions, J. High Energy Phys. 06 (2015) 102.

[22] E. Gabrielli, B. Mele, M. Raidal, and E. Venturini, FCNC decays of standard model fermions into a dark photon, Phys. Rev. D **94**, 115013 (2016).

[23] E. Gabrielli, M. Heikinheimo, B. Mele, and M. Raidal, Dark photons and resonant monophoton signatures in Higgs boson decays at the LHC, Phys. Rev. D **90**, 055032 (2014).

[24] S. Biswas, E. Gabrielli, M. Heikinheimo, and B. Mele, Dark-photon searches via Higgs-boson production at the LHC, Phys. Rev. D **93**, 093011 (2016).

[25] T. Behnke *et al.*, The International Linear Collider Technical Design Report—Volume 1: Executive summary, arXiv:1306.6327.

[26] H. Baer, T. Barklow, K. Fujii, Y. Gao, A. Hoang, S. Kanemura, J. List, and H. E. Logan *et al.*, The International Linear Collider Technical Design Report—Volume 2: Physics, arXiv:1306.6352.

[27] K. Fujii *et al.*, Physics case for the International Linear Collider, arXiv:1506.05992.

[28] M. Aicheler, M. Aicheler, P. Burrows, M. Draper, T. Garvey, P. Lebrun, K. Peach, N. Phinney *et al.*, A multi-TeV linear collider based on CLIC technology: CLIC Conceptual Design Report, Reports No. CERN-2012-007, SLAC-R-985, KEK-Report-2012-1, PSI-12-01, JAI-2012-001.

[29] FCC official Web site, https://espace2013.cern.ch/fcc/Pages/default.aspx, 2015; M. Bicer *et al.* (TLEP Design

Study Working Group), First look at the physics case of TLEP, J. High Energy Phys. 01 (2014) 164.

[30] M. Ahmad *et al.* (CEPC-SPPC Study Group), CEPC-SPPC Preliminary Conceptual Design Report, Volume I: Physics and detector, and Volume II: Accelerator, Report No. IHEP-CEPC-DR-2015-01, http://cepc.ihep.ac.cn/preCDR/volume.html, 2015.

[31] J. Alwall, R. Frederix, S. Frixione, V. Hirschi, F. Maltoni, O. Mattelaer, H.-S. Shao, T. Stelzer, P. Torrielli, and M. Zaro, The automated computation of tree-level and next-to-leading order differential cross sections, and their matching to parton shower simulations, J. High Energy Phys. 07 (2014) 079.

[32] T. Sjostrand, S. Mrenna, and P. Z. Skands, PYTHIA 6.4 physics and manual, J. High Energy Phys. 05 (2006) 026.

[33] O. Cerri, M. de Gruttola, M. Pierini, A. Podo, and G. Rolandi, Study the effect of beam energy spread and detector resolution on the search for Higgs boson decays to invisible particles at a future e^+e^- circular collider, Eur. Phys. J. C **77**, 116 (2017).

[34] T. Behnke *et al.*, The International Linear Collider Technical Design Report—Volume 4: Detectors, arXiv:1306.6329.

[35] G. Voutsinas, in FCC Week 2017, Berlin, 2017, https://indico.cern.ch/event/556692/contributions/2510761.